Journal of Physics and Chemistry of Solids 150 (2021) 109716

Contents lists available at ScienceDirect

Journal of Physics and Chemistry of Solids

journal homepage: http://www.elsevier.com/locate/jpcs

TiO_2 nano-clusters adsorbed on surfaces: A density-functional-theoretic study

F. Aguilera-Granja [a,*], R.H. Aguilera–del–Toro [b], E.E. Vogel [c,d], E. Cisternas [c]

[a] Instituto de Física, Universidad Autónoma de San Luis Potosí, San Luis Potosí, Mexico
[b] Departamento de Física Teórica, Atómica y Óptica, Universidad de Valladolid, Spain
[c] Departamento de Ciencias Físicas, Universidad de La Frontera, Temuco, Chile
[d] Center for the Development of Nanoscience and Nanotechnology (CEDENNA), 9170124, Santiago, Chile

ARTICLE INFO

Keywords:
DFT calculations
Structural properties
Electronic properties
Oxides transition metal clusters

ABSTRACT

We performed density-functional-theoretical calculations to investigate the adsorption of two stable nano-clusters corresponding to $(TiO_2)_N$ with $N = 3$ and 5 supported on three different type of substrates: graphene, silver and gold. For each of these surfaces we consider three textures: pristine, with a single vacancy and with a Co atom as impurity. In the case of the defects (vacancy or impurity) they act as possible anchors for the adsorption of the cluster. The proposed particles present flat configurations in their respective free standing putative ground states, so they can accommodate themselves as parallel, perpendicular or inclined with respect to the surface producing different isomers: only the four lowest energy isomers for each particle ($N = 3$ or 5), each surface and each texture are reported and analyzed. Density Functional Theory calculations by means of the SIESTA package are done in a thorough way covering a large number of the possible configurations. Reported parameters are: adsorption energy, assisted binding energy (binding energy in the presence of the substrate), and the main different interatomic distances presented in the adsorption. A comparison with some previous theoretical results on related systems is done. Possible extensions of this work are commented.

1. Introduction

Recent literature offers a large number of studies of free standing atomic clusters [1–6] which mostly allows for comparisons with their experimental counterparts only in the case of the gas phase, namely, in studies of their formations or fragmentation channels [7–11]. However, any possible technological application of atomic clusters requires that they are supported or embedded onto a matrix as is observed in many of the real experimental set ups [12]. Studies for supported or/and embedded clusters are much less common in the literature, although the real situation implies the presence of a substrate or a matrix. This is due to the large computational effort required to perform the calculations where substrate and/or matrix are present. Two-dimensional substrates like the graphene-like systems are more frequent in the literature [13–16] because of the simplicity to represent them due to the absence of volume. Moreover, new physical phenomena arise as a result of the low dimensionality which makes them a subject worth of numerical studies under limited conditions. We consider depositions on a finite portion of the substrate (with a large enough super-cell) leaving out of consideration depositions on semi-infinite systems which are more demanding of computing time for a correct representation. In addition, periodic boundary conditions are imposed in the usual way.

The interest for embedded atomic clusters is of long date [17], specially due to their promissory technological applications. Consequently they have been widely studied by computational approaches [18]. A particular interest has been focused on magnetic clusters because their properties are very sensitive to the structural and chemical environments [19]. Thus, Co embedded in a matrix [20], Fe embedded in a Fe–Co alloy [21] or Ni embedded in Ag [12] are some relevant examples.

Part of the present study deals with graphene-(TiO_2) where a number of experiments have been performed. Two recent review articles can serve as a general introduction to this problem [22,23]. There have also been several Density Functional Theory (DFT) calculations of studies of graphene-$(TiO_2)_N$ materials. All of them focus on smaller $(TiO_2)_N$ clusters (to mimic TiO_2 particles), in general less than few atoms in size [24,25]. Pure graphene, as well as graphene with impurities and defects have been included in these small cluster simulations. Binding energies

* Corresponding author. Universidad de Valladolid Calle Paseo de Belén, 7 47011 Valladolid, Valladolid, Spain.
E-mail address: faustino@ifisica.uaslp.mx (F. Aguilera-Granja).

https://doi.org/10.1016/j.jpcs.2020.109716
Received 14 May 2020; Received in revised form 10 August 2020; Accepted 13 August 2020
Available online 3 December 2020

of the $(TiO_2)_N$ clusters to graphene and their electronic configurations and geometrical properties (bonds) have typically been calculated in these studies. Less common are the studies of surface metal-(TiO_2) since in general the studied system have been just the opposite: a TiO_2 substrate with deposited nobel metal particles [26,27]. In this work we are mainly concerned with TiO_2 clusters on nobel metals. So far, we are not aware of similar theoretical studies.

Motivated by recent advances on depositions of TiO_2 clusters on oxides [28], conductive surfaces [29], graphene [24,25,30], silver [31] and gold [32–34] the present work is focused to the adsorption of $(TiO_2)_N$ nano-clusters on non-metallic and metallic substrates. Here N takes the values 3 and 5, which we will use to identify the clusters: $N = 3$ for $(TiO_2)_3$ and $N = 5$ for $(TiO_2)_5$.

For the non-metallic substrate we consider graphene, while two (111) surfaces are metallic substrates: Ag and Au, offering similar compact deposition surfaces. In addition, each one of them will be studied under three different conditions: pristine, single vacancy and with an atomic magnetic substitutional impurity. We have considered Co as the impurity to investigate the role played by the magnetic effects in the adsorption of the clusters.

This paper is organized as follows: after this introduction we provide details of the model and the computational procedure in Section II. Next, in Section III, we present results on the stable structures, their binding energies, adsorption energies, interatomic distances and distribution of the different pairs of the systems. Finally, in Section IV we draw conclusions and close the paper.

2. Theoretical approach and computational details

We have used the free distribution computational package SIESTA (Spanish Initiative for Electronic Simulations with Thousands of Atoms) [35] to carry out Density Functional Theory (DFT) calculations following the generalized gradient approximation (GGA) proposed by Perdew-Burke-Ernzerhof (PBE) [36]. SIESTA makes use of numerical pseudo-atomic orbitals as basis sets to solve the single particle Kohn-Sham equations. In this way the atomic cores are approximately described by nonlocal norm-conserving Troullier-Martins pseudopotentials [37] factorized in the Kleinman-Bylander form [38]. The pseudo-potentials for Ti, O, Co, Ag and Au were obtained by considering the following valence configurations $4s^2 3p^6 3d^2$, $2s^2 2p^4$, $4s^1 3d^8$, $5s^1 4d^{10}$, and $6s^1 5d^{10}$, respectively. The s, p and d cut-off radii for Ti were considered to be all equal to 1.98 a. u., the s and p radii for O are set at 1.14 a. u., the s, and d radii for Co are 2.0 a. u., the s, and d for Ag are 2.05 a. u., and the s, and d for Au been 2.46 a. u and 2.20 a. u., respectively. A double-ζ doubly polarized basis sets were employed to describe the valence states. Further details about the pseudopotentials and basis sets used for the impurities, as well as about the pertinent tests, can be found in our previous works [39–41].

All these cluster calculations were performed using periodic boundary conditions with lattice vectors large enough so the interactions between the adsorbed cluster and its replicas in neighboring cells are negligible. Thus, the shortest distances among the different images are approximately 10 Å; such distance between images originates deviations of less than 0.1% in the total energy per cluster of two free standing clusters in the gas phase. In the case of graphene a single sheet with 112 C atoms is used as substrate for the calculations with orthogonal lattice vectors (17.40 Å × 17.60 Å × 20.00 Å), where as in the case of the Ag and Au surface four layers of 30 atoms each are considered; the lower two layers are fixed to the bulk values while the upper two laters are free to relax along with the calculations. The orthogonal lattice vectors for Ag and Au are (17.15 Å × 15.45 Å × 25.00 Å) and (14.40 Å × 15.18 Å × 25.00 Å), respectively. Only the Γ-point was used for the Brillouin zone integration. We used energy cutoff of 250 R y to define the real-space grid for the electron density. We have performed several proofs to confirm the independence of the total energy values obtained in our calculations for different lattice vector sizes and energy cutoffs. For the geometric optimization of the atomic structures, we employed the conjugate gradient method [42] as implemented in SIESTA until the interatomic forces were less than 0.006 eV/Å. We performed full spin polarization calculations and full relaxation without any constrain in the optimization.

The main goal of these calculations is to minimize the assistance binding energy of the adsorbed cluster E_B^*, and the adsorption energy $E_{Ads.}$ of the supported cluster defined as follows:

$$E_B^*[(TiO_2)_N] = -\frac{E_{Total}[(TiO_2)_N + subs.] - NE_{atom}(Ti) - 2NE_{atom}(O) - E(subs.)}{3N}, \quad (1)$$

$$E_{Ads.}[(TiO_2)_N] = -[E_{Total}[(TiO_2)_N + subs.] - [E_{Total}[(TiO_2)_N] + E(subs.)]], \quad (2)$$

where "subs." means substrate, which can be any of the possible surfaces resulting from the three materials (graphene, Ag (111) or Au (111)) and the three textures for each material (pristine, vacancy or impurity). We leave out pristine graphene since it has been broadly covered in previous studies as mentioned in the Introduction. So we will work on eight different surfaces in the present work.

It is worth to quote that the assistance binding energy (E_B^*) gives us information about the energetic cost to form the complete system or separate it into its atomic parts in presence of the surface. It is important to highlight that this energy is different from the binding energy (E_B) of free standing clusters (in our case 6.208 $eV/atom$ for $(TiO_2)_3$ and 6.464 $eV/atom$ for $(TiO_2)_5$). In general, the surface plays a stabilizer role since the former (E_B^*) is 2%–6% more stable (depending of the size and type of substrate as shown in Tables 1–3) than the corresponding free standing binding energy (E_B) of the cluster. In the case of the adsorption energy, this indicates how much energy we have to pay to separate the system into its constituent parts, i.e. cluster and surface.

Previous to the deposited structures we performed our own free standing calculations for $(TiO_2)_N$ clusters ($N = 3$ and 5). The corresponding ground states are planar (2-dimensional) structures for both cases, in agreement with those reported by Juarez Da Silva and coworkers [43]. The main advantage of picking these clusters is precisely their planar shapes, which reduces the possible number of configurations adopted by the adsorbed clusters. This feature will also allow for discussions concerning the orientation of the particle with respect to the surface (parallel, perpendicular, or inclined).

3. Results

We present results for two clusters: $(TiO_2)_N$ identified as $N = 3$ and $N = 5$ deposited onto the eight possible surfaces characterized above. Co atom is used as the magnetic impurity. Results begin with structural parameters after relaxation, separating materials in subsections, and they are followed by a density of states analysis.

3.1. Energies and geometrical parameters

3.1.1. Graphene substrate

Results for $N = 3$ and $N = 5$ on a graphene sheet with a single vacancy are shown in Fig. 1. For $N = 3$ the bonding cases present two almost degenerate solutions, while for $N = 5$ these solutions are slightly different. For $N = 3$ the most stable configuration is through bonding over *O*–C atoms with an interatomic distance of 1.38 Å, adsorption energy of 2.280 eV and binding energy of 6.462 eV/atom as shown in Fig. 1a). This is followed very closely by a configuration where the binding is through Ti–C atoms, with an interatomic distance of 2.18 Å, 2.279 eV of adsorption energy and with binding energy of 6.461 eV/atom as shown in Fig. 1b) The isomer presented in Fig. 1c) is very similar to the case presented in Fig. 1b) with slightly different orientation and

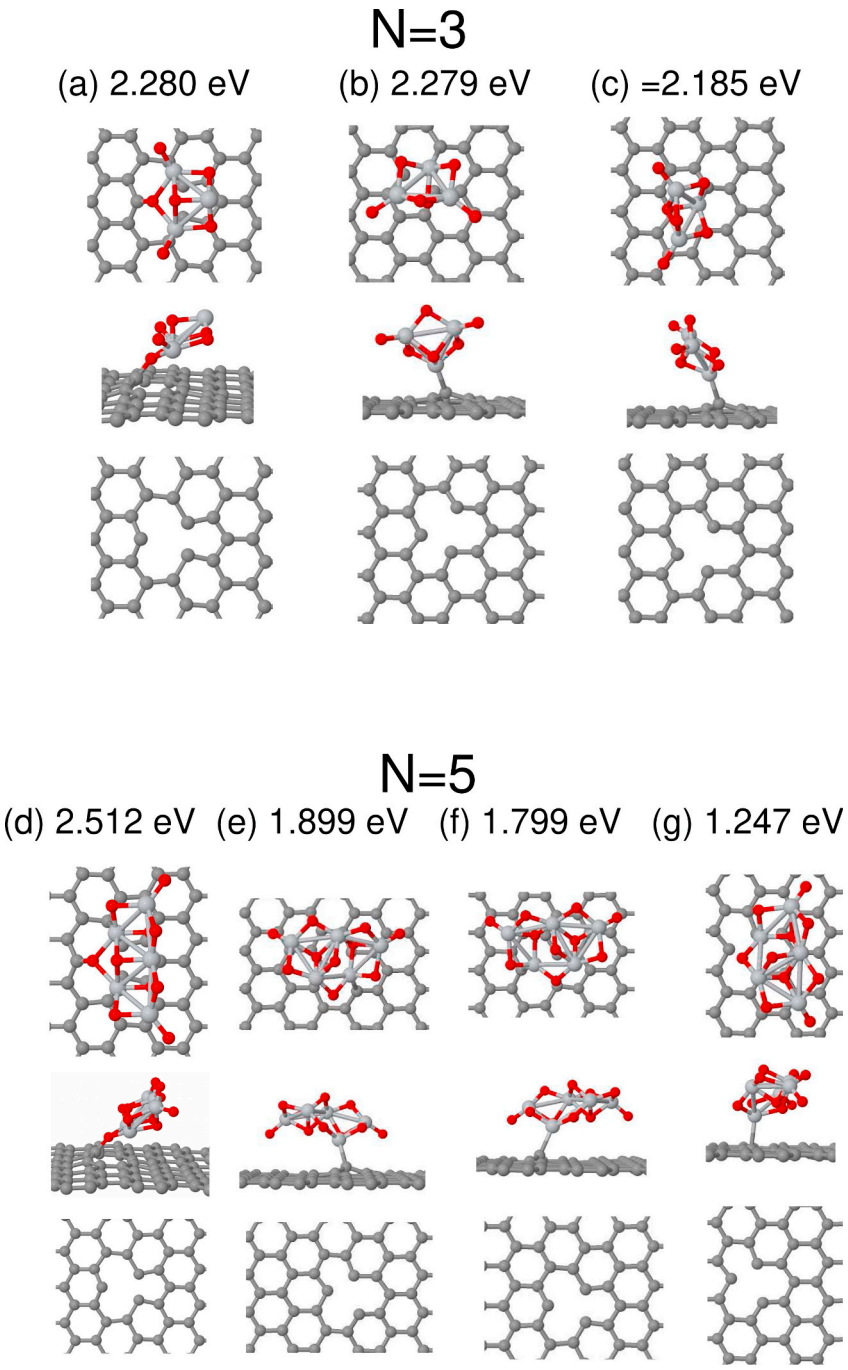

Fig. 1. Low-energy isomers adsorbed on graphene with a single site vacancy. Upper panel is for $(TiO_2)_3$ while the lower panel is for $(TiO_2)_5$. Three different views are offered for each isomer: substrate with a hole (bottom), lateral view of the deposition to appreciate bonding and inclination (middle), and top view of the deposition to appreciate orientation with respect to the geometry of the surface. The numerical value given for each isomer corresponds to its adsorption energy as defined in the text. This way of illustrating the depositions applies also to Fig. 2 through 8.

with the same interatomic distances. The interatomic distances obtained for *O*–C and Ti–C and adsorption energies reported here are in agreement with those reported by Geng, and Bukowski and coworkers [24, 25].

In the case of $N = 5$ the most stable chemi-adsorbed isomer is also through *O*–C atoms with an interatomic distance of 1.38 Å and 2.512 eV of adsorption energy and with binding energy of 6.631 eV/atom as shown if Fig. 1d). The next solutions in energy are bonding through Ti–C atoms with interatomic distances 2.17, 2.16 and 2.29 Å with adsorption energies 1.898, 1.799 and 1.247 eV and with binding energies 6.591, 6.584 and 6.547 eV/atoms presented in Fig. 1e) and f) and g) respectively. Comparison with theoretical calculations by Bukowski [25] is not fair here since the $(TiO_2)_5$ cluster used in their calculations is not the ground state [43], although the adsorption energy values are similar to ours. It is worth complementing previous information reporting that for both $N = 3$ and $N = 5$ there is a physically adsorbed solution through *O*–C bonding with a large interatomic distance of ≈ 3.2 Å and adsorption energies of ≈ 0.40 eV.

The role of the substrate in the stabilization of the adsorbed clusters can be seen through the comparison with the binding energies for the free standing clusters $N = 3$ and $N = 5$ (6.206 and 6.464 eV/atom respectively), which are slightly smaller (≈ 3.5%) than the vales reported values in presence of the graphene surface.

It is also interesting to notice that non-magnetic solutions are present for the lowest energies adsorbed clusters in general although graphene with a single vacancy has a magnetic character (with a magnetic moment of 1.42 μ_B), and that the magnetic solutions are present only for isomers far away in energy for both $N = 3$ and 5; these results are not

shown in Fig. 1 due to the large energy separation.

Results for a graphene sheet with a single Co impurity are shown in Fig. 2 for both $N = 3$ and $N = 5$. As in the case of the single vacancy the substitutional Co atom acts as anchor center for the $(TiO_2)_N$ clusters. The interatomic distances are given in Table 1 for the lower energy isomers; the number of times that the first nearest-neighbor pairs of the A-B type appears (multiplicity) in the system are given in parenthesis (A-B).

The binding energy for $N = 3$ is practically the same for the cases presented in Fig. 2a), b), c), and d) ranging from 6.398 to 6.353 eV/atom, whereas the adsorption energies show more significant changes as given in Fig. 2 itself.

In the case of $N = 5$ anchored by a Co impurity the binding energies remain close to 6.569 eV/atom only decreasing less than 0.3% in the case of the third isomer. The adsorption energies present a larger dispersion than in the case of $N = 3$ changing ≈ 20 % between the most stable (putative ground state 2(e)) and the fourth isomer (2(h)). The average energy difference due to the cluster size is ≈ 0.19 eV/atoms as shown in Table 1.

In the Co-impurity cases all solutions exhibit a localized magnetic behavior ($\approx 1.0\mu_B$) mainly due to the Co-atom. In general all adsorption energies in the case of this impurity were lower (in some cases up to $\approx 30\%$) than those corresponding to a vacancy with the same configuration. Our results indicate that the vacancy is a better anchor center

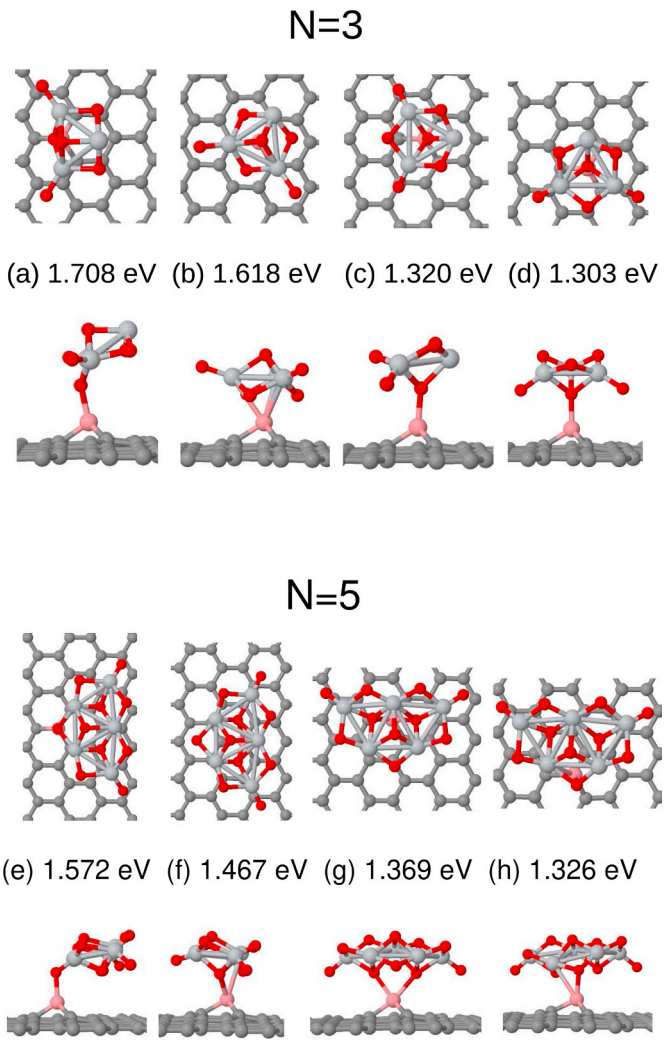

Fig. 2. Low-energy isomers adsorbed on graphene with a single Co atom as substitutional impurity. Upper panel is for $(TiO_2)_3$ while the lower panel is for $(TiO_2)_5$. The organization of the illustrations was explained in the caption of Fig. 1.

Table 1
Average interatomic distances for graphene with a Co impurity for $N = 3$ and 5, respectively. The multiplicity (number of times a bond appears in the structure) is given in parenthesis).

$(TiO_2)_3$		Co impurity	
Fig.	Isomer (E_B^* eV/atom)	O–Co Å	Ti–Co Å
2 a)	Ground state (6.398)	1.84 (1)	
2 b)	First isomer (6.388)		2.86 (3)
2 c)	Second isomer (6.355)	1.91 (1)	
2 d)	Third isomer (6.353)	1.91 (1)	
$(TiO_2)_5$			
Fig.	Isomer (E_B^* eV/atom)	O–Co Å	Ti–Co Å
2 e)	Ground state (6.569)	1.84 (1)	
2 f)	First isomer (6.562)	2.12 (2)	2.92 (2)
2g)	Second isomer (6.555)	2.11 (1)	
2h)	Third isomer (6.552)	1.94 (1)	2.80 (1)

(lower energies) than the metal impurity and that magnetism does not seem to play a relevant role in the electronic properties in the case of graphene systems.

Just to have a complementary viewpoint we also did calculations including van der Waals (VdW) interactions employing the correction DFT-D [44] as implemented in Quantum Espresso distribution [45]. As expected, we have found larger adsorption energies as compared to those without VdW. For example, in the case $N = 5$ the adsorption energy increases from 2.51 eV up to 3.42 eV when the cluster is adsorbed on a vacancy. If the same cluster is adsorbed over a Co impurity, the adsorption energy goes from 1.57 eV up to 2.78 eV. These results reflect the added interaction between dangling bonds of the graphene surface and the oxygen orbitals of the cluster. Except for some minor modulations we do not expect important changes in the relative energies among different isomers with the inclusion of VdW interactions. Clearly, such interactions are not relevant for metallic substrates.

3.1.2. *Silver substrate*

Results for the adsorption of $(TiO_2)_N$ ($N = 3, 5$) for the pristine Ag substrate, with a single vacancy and with a Co impurity are shown in Figs. 3–5, respectively. The putative ground state and the first next lowest binding energy isomers are presented showing their corresponding adsorption energies. Table 2 summarizes other results for all Ag substrates and particles organized in the following columns: reference to illustrative figure; isomer and binding energy, oxygen-substrate distance, other interatomic distances, and in parenthesis the multiplicity (number of times that a given bond appears in the system).

For depositions of $(TiO_2)_3$ over the pristine Ag substrate the lowest energy configuration is obtained when the cluster is almost orthogonal to the surface as in Fig. 3a) (Let us recall that these clusters are planar). The corresponding binding energy is 6.560 eV/atom while the adsorption energy is 3.171 eV; the bonding is through *O*–Ag pairs. As soon as the cluster adopts a configuration relatively parallel to the surface (Fig. 3b),c), and d)) the adsorption energy decreases, showing a small dependence with the orientation of the clusters. Worth noticing the binding energy is practically the same for all the planar configurations as is given in the second column of Table 2. Moreover, the average interatomic *O*–Ag distances (≈ 2.39 Å) and Ti–Ag (≈ 3.08 Å) present very similar values for the four isomers displayed in Fig. 3.

For deposition of $(TiO_2)_5$ over the pristine Ag substrate all the configurations present the plane of particle parallel to the surface as depicted in Fig. III e), f), g) and h). The binding energy is practically the same for all of them and with values for the adsorption energy that are nearly independent of the cluster direction (with deviations smaller than 6% from the average value). These binding (adsorption) energies are in general slightly larger (smaller) that the corresponding ones for $N = 3$. The general dominant bonding is through *O*–Ag pairs followed by Ti–Ag pairs; these distances are slightly larger than the corresponding ones for $N = 3$.

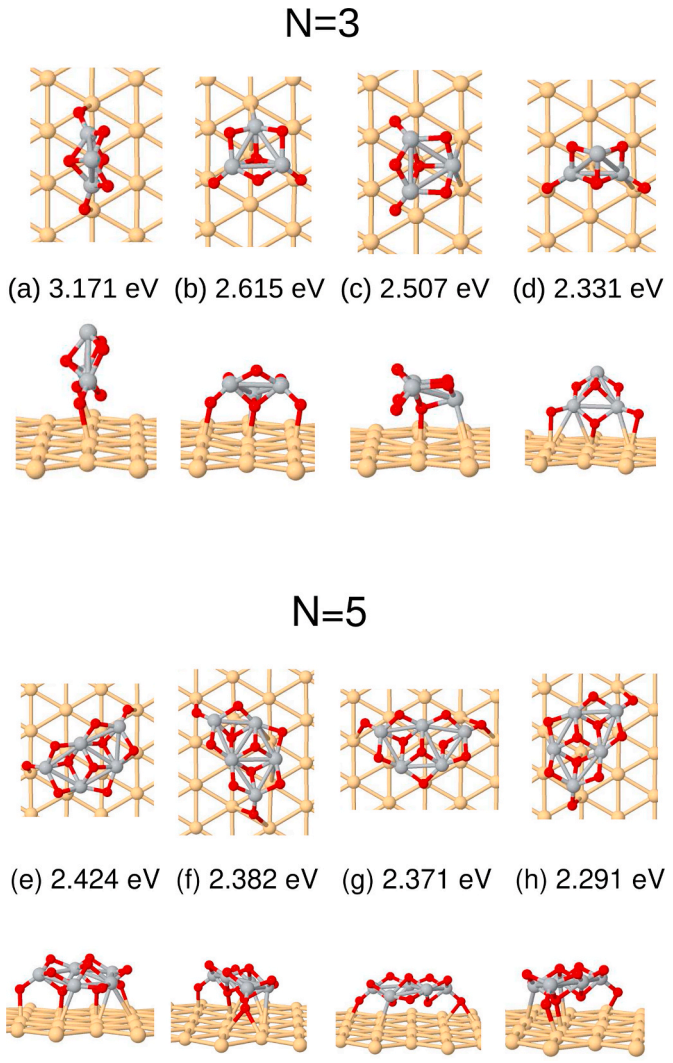

Fig. 3. Low-energy isomers adsorbed on pristine silver (111) surface. Upper panel is for $(TiO_2)_3$ while the lower panel is for $(TiO_2)_5$. The organization of the illustrations was explained in the caption of Fig. 1.

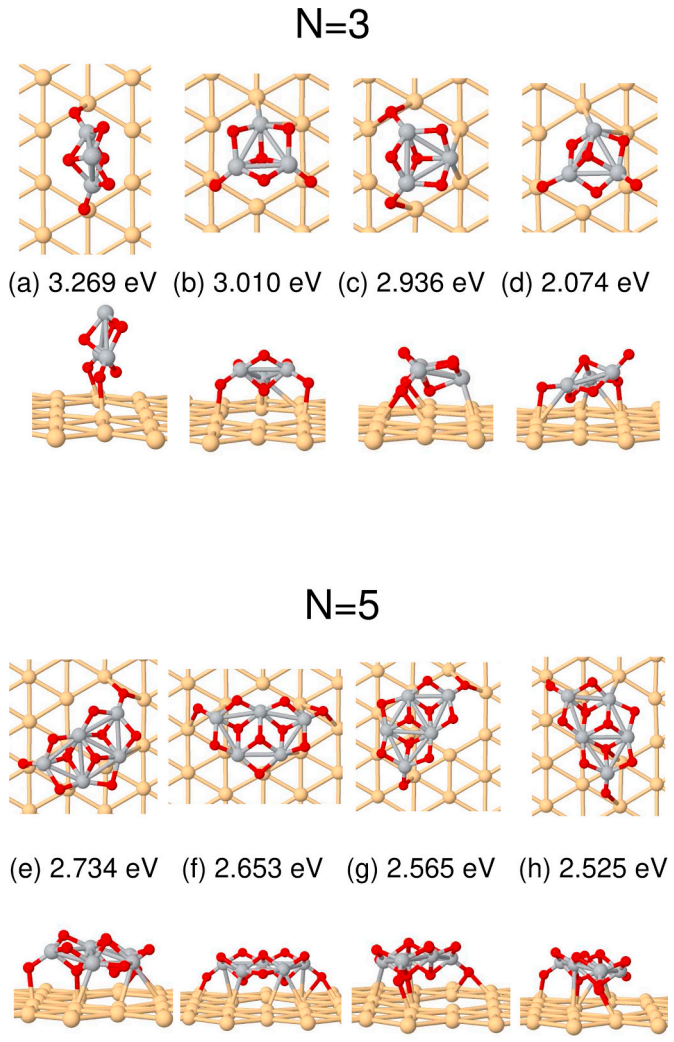

Fig. 4. Low-energy isomers adsorbed on silver (111) surface with a single site vacancy. Upper panel is for $(TiO_2)_3$ while the lower panel is for $(TiO_2)_5$. The organization of the illustrations was explained in the caption of Fig. 1.

For the Ag substrate with a vacancy the lowest energy configuration for $N = 3$ is similar to the one presented in the pristine case, namely, the adsorbed cluster is almost orthogonal to the surface directly over the vacancy as shown in Fig. 4a). Main results are summarized in Table 2. The binding energy is 6.551 eV/atom and the adsorption energy 3.269 eV. The bonding is through two *O*–Ag pairs with interatomic distances slightly smaller (2.37 Å) than the ones obtained for the pristine surface. The next three isomers adopt a configuration almost parallel to the Ag surface as shown in Fig. 4b), c), and d), as the adsorption energy decreases over 0.25 eV; orientation changes are observed in this series. The binding energies show very little dispersion (differences are within 0.1 eV/atom) as it can be appreciated from Table 2. As in the pristine case both *O*–Ag and Ti–Ag pairs are separated with very similar distances in all the cases and shorter interatomic distances as compared to the pristine case, as it can be expected.

Similarly to what was found for the pristine surface for $N = 5$ the main four configurations are parallel to the surface (see Fig. 4e) and f), g) and h)) with practically the same binding energy for all clusters, almost independent of their directions. Adsorption energies present stronger direction dependence than the in the pristine case with deviations as large as 8%. The binding and adsorption energies are in general slightly larger that the ones for $N = 3$ for the putative ground state and the first two isomers. The dominant bonding pairs are *O*–Ag in general followed by Ti–Ag, whereas the former resembles very much the corresponding case for $N = 3$ while the latter comes out only slightly larger than for $N = 3$.

We report now results for depositions over Ag substrate mediated by Co impurity atoms. The main energy configurations for $N = 3$ are presented in Fig. 5a) and b), c) and d), with a summary of properties given in Table 2. The two lowest energy configurations are those with the central O of the cluster over the Co impurity; they are practically degenerate showing a binding energy difference of only 0.01 eV/atom. The adsorption can be established by means of all possible pairs, namely; in the case of adsorption energy the difference between the putative ground and the first isomer is less than 0.1 eV. For these clusters all possible atomic pairs are relevant, namely *O*–Ag, Ti–Ag, O–Co and Ti–Co, as it is shown in Table 2. The shortest average interatomic distance is for O–Co pairs nearly at 2.0 Å, followed by *O*–Ag pairs at ≈ 2.4 Å; distances for Ti–Co and Ti–Ag pairs reach even larger values: 2.75 Å, and 2.96 Å, respectively.

The configurations for $N = 5$ are presented in Fig. 5e) and f), g) and h), with the corresponding properties listed in the lower part of Table 2. All these configurations are parallel to the surface with practically the same binding energy (differences are in the range of 0.025 eV/atom) and with some dependence of the adsorption energy with both the cluster orientation over the surface and the relative position of the Co-impurity with respect to the adsorbed cluster, showing differences in the range of

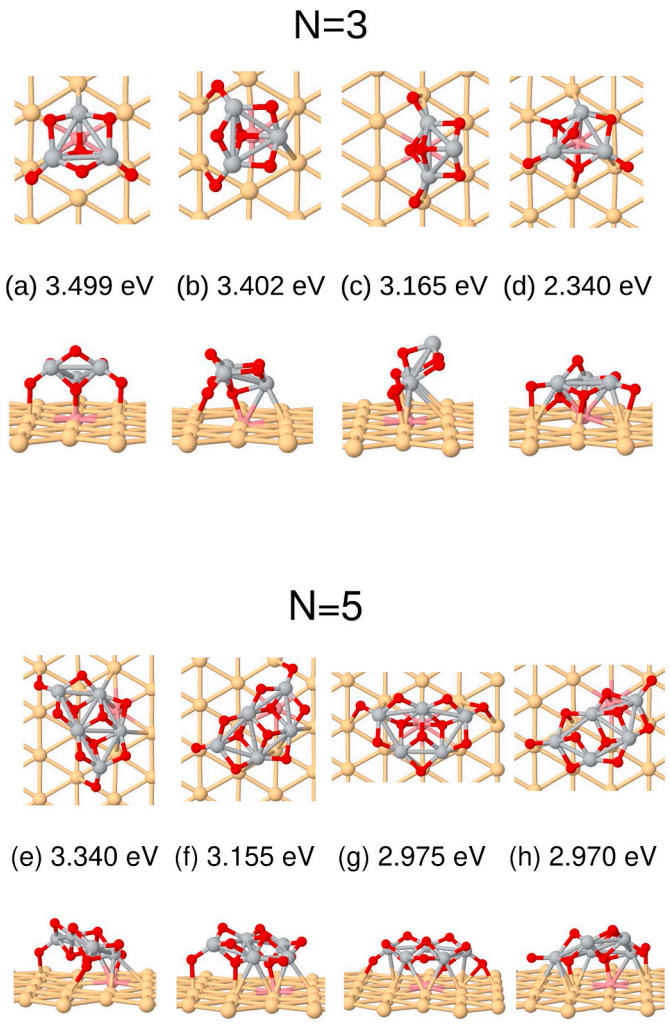

Fig. 5. Low-energy isomers adsorbed on silver (111) surface with a single Co atom as substitutional impurity. Upper panel is for $(TiO_2)_3$ while the lower panel is for $(TiO_2)_5$. The organization of the illustrations was explained in the caption of Fig. 1.

0.37 eV. The lowest energy configuration is nearly symmetric for a mirror going over the Co, Ti and two O atoms. All type of pairs are present in the adsorbed configurations with values very similar to the ones for the $N = 3$ case. The binding (adsorption) energies are in general slightly larger (smaller) that the corresponding ones for $N = 3$.

For the case of the silver surface the largest adsorption energies are generally presented by the impurity case followed by the vacancy (hole case) and finally the pristine case as it can be expected. The energy values are practically the same for the pristine and the impurity case (differences are within 0.05 eV/atoms) independent of the cluster size.

It is worth to consider that the importance of Ag–O pairs has recently been studied in SiO_2 substrates with Ag nanoparticles, finding that these pairs (Ag–O) play a fundamental role in the oxidation of CO molecules [27]. Our study shows that Ag–O pairs also play an important role in the adsorption of the TiO_2 cluster on Ag (111) substrates.

3.1.3. Gold substrate

The presentation of results for deposition of $(TiO_2)_N$ clusters over the (111) surface of gold mirrors the just presented one for Ag as it can be appreciated in Figs. 6–8, and Table 3.

The lowest binding energy configurations for $N = 3$ over a pristine (111) Au substrate are presented in Fig. 6a) and b), c) and d), while the main properties are summarized in the upper part of Table 3. The lowest

Table 2
Main results for $(TiO_2)_N$ depositions over Ag (111), separated according to the three possible textures. First column identifies the isomer relating it to the corresponding figure; Second column labels the isomer and gives the binding energy in eV; Third through sixth columns give interatomic distances in the following order: *O*–Ag, Ti–Ag, O–Co and Ti–Co; multiplicities of each bond are given in parenthesis.

$(TiO_2)_3$		Pristine			
Fig.	Isomer (E_B^* eV/atom)	*O*–Ag Å	Ti–Ag Å		
3a)	Ground state (6.560)	2.44 (2)			
3b)	First isomer (6.499)	2.38 (3)	3.02 (2)		
3c)	Second isomer (6.486)	2.31 (1)	3.00 (2)		
3d)	Third isomer (6.467)	2.42 (3)	3.21 (3)		
$(TiO_2)_5$					
Fig.	Isomer (E_B^* eV/atom)	*O*–Ag Å	Ti–Ag Å		
3e)	Ground state (6.626)	2.40 (4)	3.12 (3)		
3f)	First isomer (6.623)	2.40 (3)	3.14 (3)		
3g)	Second isomer (6.622)	2.44 (3)	2.97 (1)		
3h)	Third isomer (6.616)	2.39 (3)	3.08 (2)		
$(TiO_2)_3$		**Vacancy**			
Fig.	Isomer (E_B^* eV/atom)	*O*–Ag Å	Ti–Ag Å		
4a)	Ground state (6.551)	2.37 (2)			
4b)	First isomer (6.542)	2.31 (2)	3.00 (2)		
4c)	Second isomer (6.534)	2.48 (4)	2.91 (2)		
4d)	Third isomer (6.439)	2.39 (2)	3.12 (3)		
$(TiO_2)_5$					
Fig.	Isomer (E_B^* eV/atom)	*O*–Ag Å	Ti–Ag Å		
4e)	Ground state (6.646)	2.38 (4)	3.03 (3)		
4f)	First isomer (6.641)	2.44 (3)	3.12 (5)		
4g)	Second isomer (6.635)	2.37 (4)	3.02 (2)		
4h)	Third isomer (6.632)	2.40 (4)	3.23 (3)		
$(TiO_2)_3$		**Co impurity**			
Fig.	Isomer (E_B^* eV/atom)	*O*–Ag Å	Ti–Ag Å	O–Co Å	Ti–Co Å
5a)	Ground state (6.597)	2.33 (2)	2.79 (1)	2.01 (1)	2.59 (1)
5b)	First isomer (6.586)	2.47 (2)	2.93 (2)	1.97 (1)	2.74 (1)
5c)	Second isomer (6.560)	2.40 (2)	3.10 (4)	1.90 (1)	2.96 (2)
5d)	Third isomer (6.468)	2.40 (4)	3.00 (4)	2.11 (2)	2.67 (3)
$(TiO_2)_5$					
Fig.	Isomer (E_B^* eV/atom)	*O*–Ag Å	Ti–Ag Å	O–Co Å	Ti–Co Å
5e)	Ground state (6.687)	2.40 (2)	3.08 (4)	2.00 (1)	2.65 (2)
5f)	First isomer (6.674)	2.35 (3)	3.03 (4)	1.97 (1)	
5g)	Second isomer (6.662)	2.44 (3)	3.11 (6)	2.15 (2)	
5h)	Third isomer (6.662)	2.46 (2)	3.07 (6)	1.95 (1)	2.81 (1)

energy configuration has the cluster in a position almost orthogonal to the surface (similarly to what was already reported for the pristine Ag surface), with a binding energy of 6.424 eV/atom; the adsorption energy is 1.949 eV as reported in Fig. 6a). Next adsorbed isomers adopt a configuration parallel to the surface, with adsorption energies decreasing for the next isomers, which at the same time change their relative orientation. The binding energies of the leading two isomers are very similar as presented in Table 3. The bonding is mainly through *O*–Au pairs presenting average distances *O*–Au of ≈ 2.51 Å, while the binding through Ti–Au pairs are present only in the parallel configurations all of them with average distance of ≈ 2.90 Å.

Similar depositions for $N = 5$ present low energy configurations favoring orientations parallel to the surface as illustrated in Fig. 6e) and f), g), and h) with additional information reported in Table 3. Binding energy presents very little dispersion (in average $\approx$ 6.536 eV/atom),

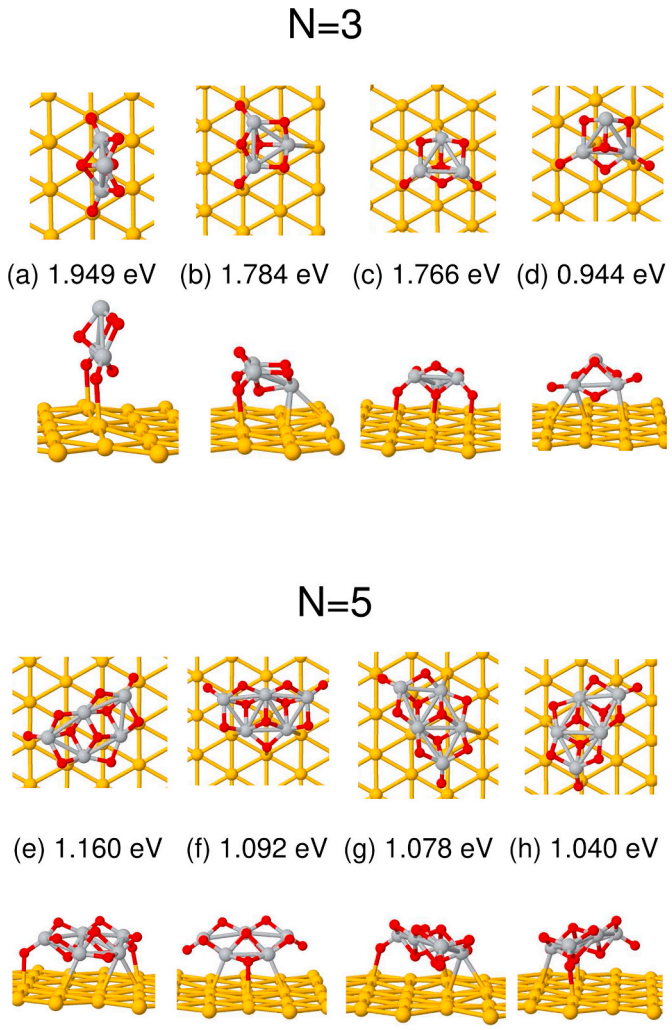

Fig. 6. Low-energy isomers adsorbed on pristine gold (111) surface. Upper panel is for $(TiO_2)_3$ while the lower panel is for $(TiO_2)_5$. The organization of the illustrations was explained in the caption of Fig. 1. (For interpretation of the references to colour in this figure legend, the reader is referred to the Web version of this article.)

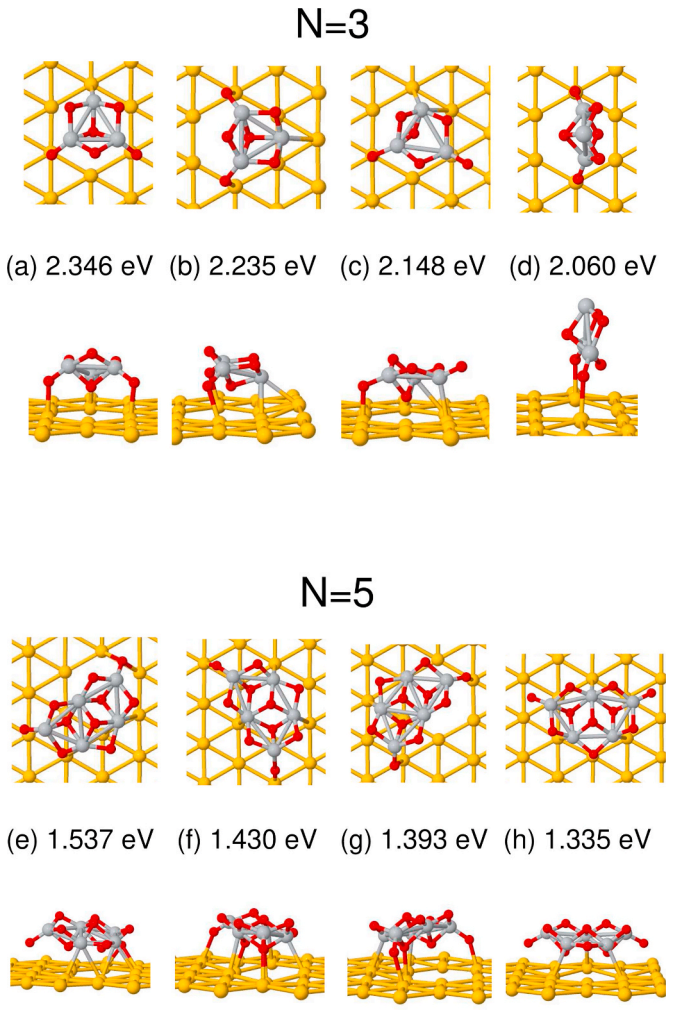

Fig. 7. Low-energy isomers adsorbed on gold (111) surface with a single site vacancy. Upper panel is for $(TiO_2)_3$ while the lower panel is for $(TiO_2)_5$. The organization of the illustrations was explained in the caption of Fig. 1. (For interpretation of the references to colour in this figure legend, the reader is referred to the Web version of this article.)

while adsorption energies vary in about 12% according to the preferred orientation. Binding (adsorption) energies are in general larger (smaller) than the corresponding ones for $N = 3$. The dominant bonding pairs are Ti–Au, followed by the *O*–Au. The Ti–Au (*O*–Au) distances are slightly larger (smaller) than those for the case $N = 3$,

If we compare the depositions for $(TiO_2)_N$ ($N = 3$ and 5) over Au (111) with those on Ag (111), we find that binding energies are lower for gold than for silver substrates, adsorption energies are notoriously lower for Au than for Ag, noble metal-oxygen distances are larger for Au than for Ag, and noble metal-Ti distances tend to be smaller for Au than for Ag but with a mixed behavior.

The lower energy configurations for depositions of $(TiO_2)_3$ on a Au (111) substrate with a vacancy are given in Fig, 7 a), b), c), and d) complemented by data in Table 3. In deep contrast to what was found for the Ag substrate the lowest energy isomer presents a deposition parallel to the surface with a binding energy of 6.469 eV/atom and an adsorption energy of 2.346 eV. It is only for third isomer over this configuration (with a difference of 32 meV/atom with respect to previous one) that we find the perpendicular deposition that was the putative ground state for the vacant Ag site. The difference in deposition energy between the ground state (Fig. 7a) and the perpendicular deposition is of 286 meV. The leading three isomers are basically parallel to the surface modulated by slightly different orientations. The main bonding is through two *O*–Au pairs with interatomic distances smaller than those corresponding to the pristine surface (2.34 Åfor the ground state). Generally speaking these *O*–Au and Ti–Au distances are shorter than the interatomic distances for the pristine case as it can be expected.

The most important configurations for $N = 5$ are presented in Fig. 7e) and f), g), h) with additional information in Table 3. The preferred orientation is parallel to the surface and the binding energies are slightly larger ($\approx$ 6.56 eV/atom) than for the pristine case with very small dispersion. The deposition energies show a slightly larger direction dependence than in the pristine case with deviations as large as the 15%. The dominant bonding pairs are for Ti–Au followed by *O*–Au pairs being the former generally larger than those for $N = 3$ and the latter only slightly larger than those.

The low-energy configurations for $N = 3$ in the case of Au substrate with an Co impurity are shown in Fig. 8a), b), c), and d), while complementary numerical data are listed in Table 3. The first two isomers differ only in 0.01 eV/atom in binding energy, they are parallel to the surface with the central O atom just over the Co impurity. Adsorption energies are only $\approx$ 0.1 eV appart. Next two isomers present less parallelism to the surface with adsorption energies decreasing (see c) and d)). For the putative ground state almost all the different types of pairs are present (*O*–Au, Ti–Au, O–Co and Ti–Co) as is shown in Table 3;

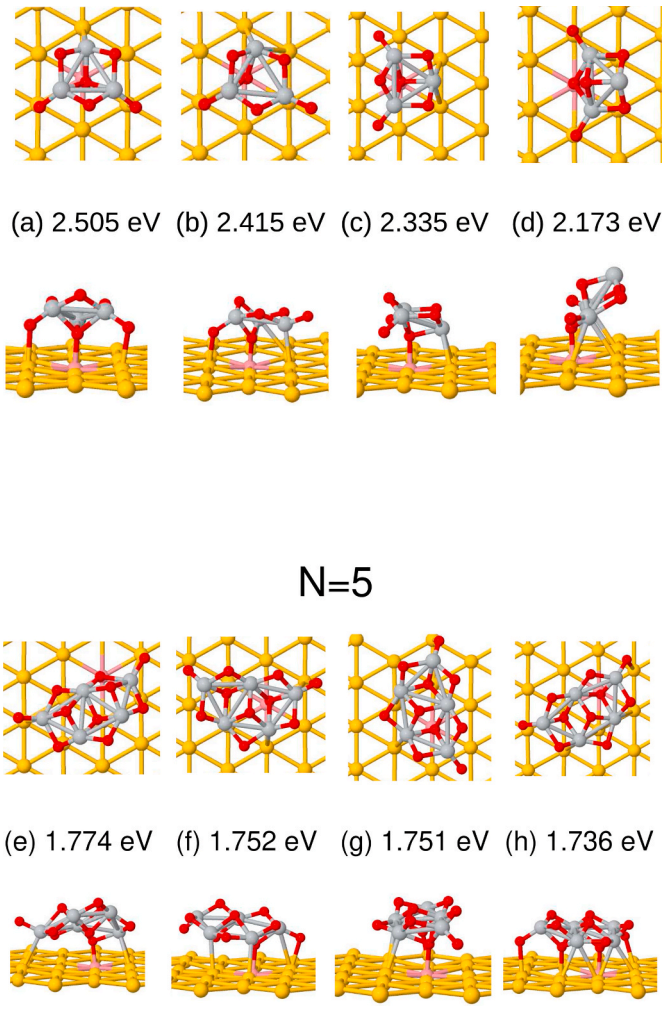

Fig. 8. Low-energy isomers adsorbed on gold (111) surface with a single Co atom as substitutional impurity. Upper panel is for $(TiO_2)_3$ while the lower panel is for $(TiO_2)_5$. The organization of the illustrations was explained in the caption of Fig. 1. (For interpretation of the references to colour in this figure legend, the reader is referred to the Web version of this article.)

the same Table also reports the distances for the main pairs of the other isomers. Generally speaking, O–Co pairs present the shortest distances (≈ 2.0 Å), followed by *O*–Au pairs, then by Ti–Au pairs, ending with Ti–Co pairs (3.06 Å) which has the particular feature of being present in the putative ground state only.

Fig. 8e), f), g), and h) and lower part of Table 3 summarize the properties of the four lowest energy isomers for $N = 5$ deposited over a Au substrate with a Co impurity. All these configurations are parallel to the surface with practically the same binding energy (≈ 6.58 eV/atom). Adsorption energy present less dispersion than in other previous cases in spite of clear different orientations and on the relative position of the Co-impurity with respect to the adsorbed cluster (differences are in the range of 40 meV). The lowest energy configuration is non-symmetric with respect to the Co impurity position. Actually, the configuration with the Co impurity at the symmetry center is way out of the binding energy range of these 4 isomers (≈ 6.541 eV/atom) and adsorption energy also quite different (1.181 eV). O–Co are the main bonding pairs with interatomic distances of about 2 Å. On the other extreme Ti–Co pairs are not present in the low-energy adsorbed isomers for this substrate.

Just quickly reviewing results for the metallic substrates we can generally say that the larger binding energies occur for the Co impurity case, followed by the vacancy on the surface, leaving the pristine case as the surface with the less bound deposited particles.

Table 3
Main results for $(TiO_2)_N$ depositions over Au (111), separated according to the three possible textures. First column identifies the isomer relating it to the corresponding figure; Second column labels the isomer and gives the binding energy in eV; Third through sixth columns give interatomic distances in the following order: *O*–Au, Ti–Au, O–Co and Ti–Co; multiplicities of each bond are given in parenthesis.

$(TiO_2)_3$		Pristine			
Fig.	Isomer (E_B^* eV/atom)	*O*–Au Å	Ti–Au Å		
6a)	Ground state (6.424)	2.61 (2)			
6 b)	First isomer (6.406)	2.45 (2)	2.97 (3)		
6c)	Second isomer (6.404)	2.46 (3)	2.71 (1)		
6d)	Third isomer (6.313)	2.51 (1)	3.03 (3)		
$(TiO_2)_5$					
Fig.	Isomer (E_B^* eV/atom)	*O*–Au Å	Ti–Au Å		
6e)	Ground state (6.541)	2.47 (2)	3.02 (3)		
6f)	First isomer (6.537)	2.56 (1)	2.89 (2)		
6g)	Second isomer (6.536)	2.46 (1)	3.07 (3)		
6h)	Third isomer (6.533)	2.41 (1)	2.90 (2)		
$(TiO_2)_3$		**Vacancy**			
Fig.	Isomer (E_B^* eV/atom)	*O*–Au Å	Ti–Au Å		
7a)	Ground state (6.469)	2.34 (2)	2.64 (1)		
7 b)	First isomer (6.456)	2.35 (2)	2.92 (3)		
7c)	Second isomer (6.446)	2.21 (1)	2.89 (3)		
7d)	Third isomer (6.437)	2.50 (2)			
$(TiO_2)_5$					
Fig.	Isomer (E_B^* eV/atom)	*O*–Au Å	Ti–Au Å		
7e)	Ground state (6.567)	2.45 (2)	3.03 (4)		
7f)	First isomer (6.559)	2.46 (4)	2.95 (3)		
7g)	Second isomer (6.556)	2.45 (3)	2.89 (2)		
7h)	Third isomer (6.553)		2.94 (3)		
$(TiO_2)_3$		**Co impurity**			
Fig.	Isomer (E_B^* eV/atom)	*O*–Au Å	Ti–Au Å	O–Co Å	Ti–Co Å
8a)	Ground state (6.486)	2.42 (2)	2.66 (1)	2.07 (1)	3.06 (1)
8 b)	First isomer (6.476)	2.30 (1)	2.93 (3)	1.95 (1)	
8c)	Second isomer (6.467)		2.83 (2)	2.07 (1)	
8d)	Third isomer (6.449)		3.00 (4)	1.90 (1)	
$(TiO_2)_5$					
Fig.	Isomer (E_B^* eV/atom)	*O*–Au Å	Ti–Au Å	O–Co Å	Ti–Co Å
8e)	Ground state (6.582)		2.97 (4)	1.98 (1)	
8f)	First isomer (6.581)	2.39 (1)	2.97 (3)	2.05 (1)	
8g)	Second isomer (6.580)	2.45 (2)	2.91 (3)	2.04 (1)	
8h)	Third isomer (6.579)	2.44 (3)	3.01 (4)	2.01 (1)	

It is worth commenting that atomic experimental embodiments in the case of TiO_2 clusters on Au (111) have been reported [32,33]. Although the supported clusters are very large for a direct comparison with our calculations, it is important to notice that the experiments report deformations (tensile-strained) in the TiO2 nano-crystals [32]; this is in line with our results where slight local distortions (deviations of ± ≈ 2%) in the Ti–Ti bonds of the nano-cumulers are observed with respect to the free standing nanoclusters, thus abandoning the flat shape of these free standing nano-clusters. It has also been reported experimentally that the Au–O bonds of stoichiometric TiO_2 (deposited on the substrate) are essential for the creation of active sites for dissociating H_2 [46]; this effect has also been observed for ethanol, Co and O_2[47,48] Our calculation show that the leading bond in the adsorption of TiO_2--nanoclusters are precisely the Au–O bonds as show in Table 3. This is

also observed in our results for the Ag (111) substrate as shown in Table 2.

3.2. Electronic density of sates

Now we will present the results of the Density of States (DOS), and in order not to make the discussion very repetitive we will only present the results of the case $(TiO_2)_5$ over some of the substrates here considered, althoug we have all the cases.

The corresponding DOS functions for the different species of $(TiO_2)_5$ deposited over graphene with a vacancy are presented in Fig. 9. Total DOS is represented by widest line in every panel. The upper and central panels show the corresponding isolated systems (without interaction): cluster and substrate respectively. It is possible to appreciate the asymmetry between up and down bands evidencing the magnetic behavior due to the C dangling bonds. In the case of the supported system (lower panel) we can see a shift in energy levels towards less negative values and more mixing with respect to the free standing cluster of the Ti and O orbitals as a consequence of the substrate and cluster interaction. The bands associated with graphene are considerably wider than the energetic spectrum of the titanium dioxide cluster. The graphene substrate loses the magnetic character as a consequence of the adsorbed cluster, as it can be observed in the symmetric behavior of the up and down bands in the lower panel. The $(TiO_2)_5$ cluster on this substrate shows a well defined insulator-like behavior with a gap similar to the free standing case. The entire system [$(TiO_2)_5$ + graphen] shows an evidencing a narrow gap semiconductor or even a semi-metal mainly due to the C-atoms.

The corresponding Density of States (DOS) functions for the $(TiO_2)_5$ over graphene with a Co-impurity are presented in Fig. 10. The upper and central panels show the corresponding isolated systems for the cluster and substrate respectively (with clear magnetic behavior due to the Co-impurity). The total DOS is presented in every panel with the widest line. In the case of the supported system (lower panel) we can see a shift in energy levels towards negative values and mixing of the Ti, O and Co orbital in the entire range of energy values of the $(TiO_2)_5$ as a consequence of the substrate. As in the vacancy case the graphene bands are wider than the ones of the titanium dioxide. The electronic Co levels are clearly observed in the entire range of energy values of the titaniun dioxide cluster, and also over the ocupated Oxigen states (previous HOMO in the free standing cluster) between −2.0 eV and the Fermi level. The graphene substrate keeps the marginal magnetic character after the adsorption of the cluster; this effect is observed in the weak asymmetric behavior in the up and down bands presented in the lower panel. The $(TiO_2)_5$ cluster over this substrate shows almost a vanishing gap or weak insulator behavior formed mainly by the Ti electrons, the former evidence a narrow gap semiconductor or even a semimetal.

We very briefly summarize the main results for Ag substrates with the deposition of $(TiO_2)_5$ clusters. The electronic states of the titanium dioxide are within the same range of energy values of the Ag substrate for all cases. Larger mixing of orbitals is observed for the supported cluster as compared to the free-standing one due to the substrate-cluster interaction. A well defined band for the titanium dioxide is formed in all cases and in higher degree in the Co-impurity case. Metallic-like character is observed in the $(TiO_2)_5$-substrate system for the three cases here considered, being the Ti electrons the responsible ones for this behavior for the pristine and the vacancy cases. Both Ti and Co contribute in the impurity case. The corresponding Density of States (DOS) for the $(TiO_2)_5$ over the Ag substrate in the pristine and in the one Co-impurity case are presented in Fig. 11 in the top and in the bottom panels, respectively. In the pristine case a non magnetic solution is observed whereas in the impurity case a marginal magnetic behavior is observed in the system mainly from the Co-bands. Notice that a larger mixing in the electronic orbitals is more notorious in the impurity case as compared to the pristine system.

Similar results to those just presented for Ag are found for the corresponding three cases of the Au substrate. For the sake of simplicity and space considerations we omit the detailed presentation.

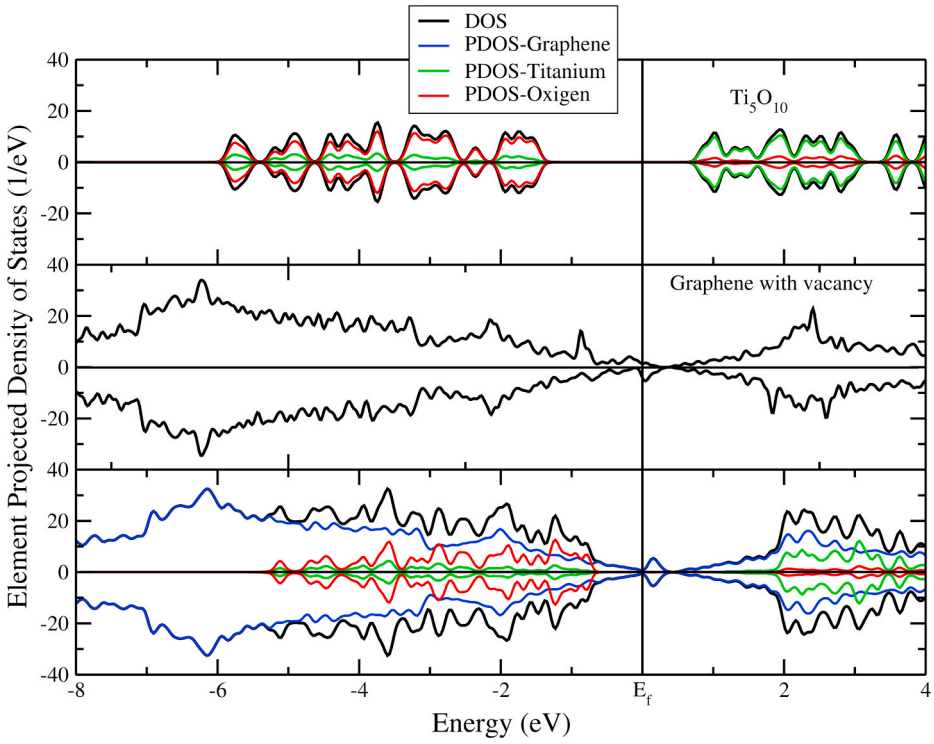

Fig. 9. DOS for the isolated $(TiO_2)_5$ cluster (top), the substrate with a single vacancy (middle), and the cluster deposited on this substrate (bottom). Different contributions to the total DOS function (widest line) are defined in the inset.

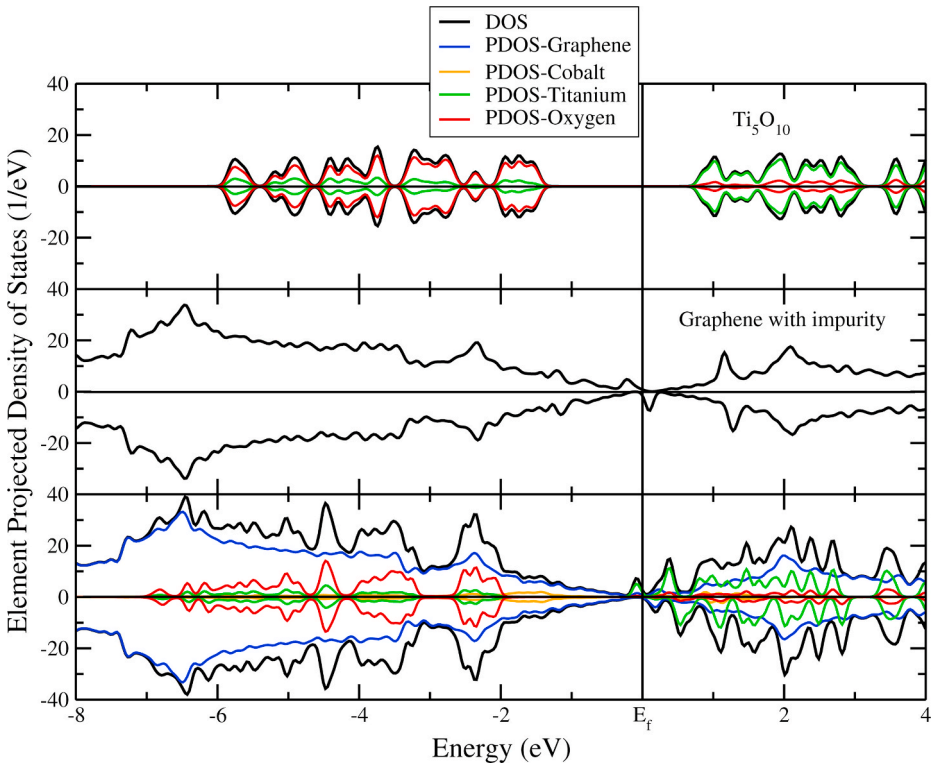

Fig. 10. DOS for the isolated $(TiO_2)_5$ cluster (top), the substrate with a single Co atom as substitutional impurity (middle), and the cluster deposited on this substrate (bottom). Different contributions to the total DOS function (widest line) are defined in the inset.

4. Conclusions

Two titanium dioxide clusters are tested for stable depositions onto nonmetallic (graphene) and metallic (Ag (111) and Au (111) surfaces) surfaces. In the metallic cases three textures are considered: pristine, single site vacancy and single magnetic (Co) substitutional atom. For graphene only the last two surfaces are reported here. The free-standing ground configurations for $(TiO2)_N$ (with $N = 3$ and $N = 5$) clusters are both flat, which allows to minimize the relative particle-surface positions. The main general conclusions of this work are two-fold: on one hand, these 2 clusters over 8 textures offer a large variety of possible ground deposited configurations, each one with a corresponding family of next metastable isomers; on the other hand, textures lead to some general trends for the properties of these systems.

The specific properties for each of the 16 different systems (2 particles and 8 textures) were already discussed in the text, illustrated by figures and summarized in tables. At this point we proceed to highlight some of the particular cases which serve as examples of some particular properties. We begin by structural properties ordered by surface material (graphene, silver and gold) followed by some remarks on the density of states for $(TiO2)_5$.

In the case of graphene with a single vacancy the putative ground state these $(TiO2)_N$ clusters tend to be adsorbed slightly tilted to the surface; bonding goes through a single O-atom. Similar behavior is observed in the case of the graphene with a Co impurity. Multiple bonding appear for some of the low-energy isomers in the graphene with Co-impurity.

The largest adsoption energy for graphene is for the vacancy case, regardless of the $(TiO_2)_N$ cluster size. The bonding for the putative ground state in the case of graphene with vacancy is through O atoms with *O*–C distances of ≈ 1.38 Å followed by the Ti–O bonds with distances of ≈ 2.2 Å. In the case of the Co-impurity the putative ground state bonding is through O–Co bonds covering distances in the range of ≈ 1.84–2.11 Å in this case the Ti–Co bond is of ≈ 2.86 Å.

Generally speaking, the putative ground configurations for Ag (111) and Au (111), lead to clusters nearly parallel to the substrate surface, with the exceptions of $(TiO2)_3$ on both pristine silver and gold, as well as on silver impurity substrate. This parallel tendency continues to the low-energy isomers, with the exception of $(TiO_2)_3$ in Au (111) with vacancy, where a higher energy configurations shows an almost perpendicular orientation with respect to the surface. For both metallic substrates the adsorption energies tend to grow in the sequence pristine, vacancy impurity.

In general, binding energies for the deposited clusters are larger for $(TiO_2)_5$ than for $(TiO_2)_3$ through the different metallic textures. For each cluster larger binding energies correspond to the impurity case. Vacancy surface produces slightly larger binding energies than the pristine case for $(TiO_2)_5$, while they are alike and mixed for $(TiO_2)_3$. The dispersion of binding energies through the calculated isomers is similar for both clusters in pristine and vacancy metallic surfaces, while it is larger for Co impurity surfaces.

Different types of bondings are presented in the clusters configurations over the metallic surfaces (O-Metal, Ti-Metal; and also O-Imp. and Ti-Imp for the impurity texture). The interatomic distances in the Ag case are ≈ 2.4 and 3.0 Å for the *O*–Ag and Ti–Ag, respectively; for the impurity texture the distances O–Co and Ti–Co are ≈ 2.0 and 2.7 Å respectively. For the case of depositions on Au (111) Interatomic distances corresponding to the depositions of these same cluster on Au surfaces are only slightly larger than those in Ag (111), following similar trends. Larger differences are found in the adsorption energies since they are about 50% smaller in Au (111) substrate as compared to the Ag case, which is due to the larger reactivity of silver surfaces.

The DOS of the graphene with vacancy produces asymmetric spin bands giving local magnetism due the dangling bonds. However, the presence of the cluster readily saturates all bonds, recovering the magnetic neutrality of the system and leaving local states near the Fermi level.

The DOS of the graphene with Co impurity produces more notorious

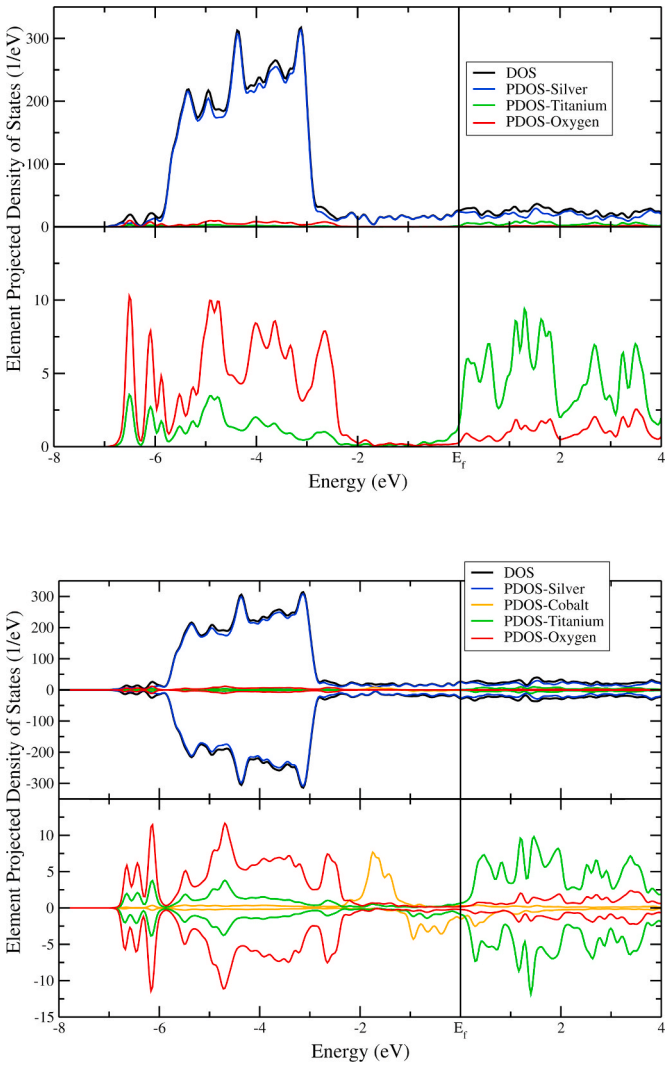

Fig. 11. DOS for the $(TiO_2)_5$ cluster on pristine silver (111) surface (upper panel) and on silver (111) surface with a single Co atom as substitutional impurity (lower panel). Different contributions to the total DOS function (widest line) are defined in the inset of each panel.

asymmetric spin bands giving local magnetism due the Co orbitals. The presence of the cluster cannot eliminate this source of magnetism which prevails to some extent. Localized electronic states are to be found near the Fermi level and Co also contributes to the conduction band.

In general, we can see that in the case of clusters deposited onto metallic substrates there are no important differences among isomers (including the putative ground state) as compared to the case of clusters deposited on graphene. The difference seems to relay on the nature of the bonding to the surface which for the latter is provided by the localized orbitals of the carbon which are ready to accept electrons from the cluster. In the metallic surface there are no such rigid bonds and the energy can be more relaxed within the cluster itself, so it is quite similar among the different isomers.

The present calculation can be helpful to understand the experimental results that are performed of nanodispersed two dimensional TiO_2 nanocrystallites on nobel metals [34], and it is also ideal system to mimic the enhanced catalytic reactivity of supported nobel metals (Ag, Au, Pt, etc.) nanoparticles. A possible natural extension of this work would be to study the adsorption and/or dissociation of H_2, CO and CO_2 at active sites in the vicinity of the noble metal (Ag and Au) and the Oxygen atoms of the TiO_2 nanoclusters as reported experimentally [46–48].

Author statement

F. Aguilera-Granja: Calculation, analysis and discussion, writing and design of figures. R.H. Aguilera–del–Toro: Calculation, discussion, and design of figures. E.E. Vogel: Structure and presentation of the paper, analysis and discussion, writing and style correction, modifications of the figures. E. Cisternas: Calculation and discussion.

Declaration of competing interest

The authors declare that they have no known competing financial interests or personal relationships that could have appeared to influence the work reported in this paper.

Acknowledgments

We aknowledge the comments and discussions with Prof. A. Vega and L.C. Balbas. R.H.A.T acknowledges financial support from the Universidad de Valladolid (spain) for the postdoctoral contract (contract number E-47-2019-0197368). E.V. and E.C. acknowledge support from the following Chilean sources is acknowledged: Fondecyt (Chile) under contract 1190036, and Financiamiento Basal para Centros Científicos y Tecnológicos de Excelencia (Chile) through the Center for Development of Nanoscience and Nanotechnology (CEDENNA, Conicyt Contract AFB180001) and to the Millenium Nucleus MultiMat. We also acknowledge to José Limón (IF-UASLP in México) and Diego Lasa (DIPC in San Sebastián, Spain) for its invaluevel computational support.

References

[1] I.M. Bilas, A. Châtelain, W.A. de Heer, Science 265 (1994) 1682–1684.
[2] F. Aguilera–Granja, J.L. Rodríguez–López, K. Michaelian, E.O. Berlanga–Ramírez, A. Vega, Phys. Rev. B 66 (2002) 224410.
[3] J.L. Rodríguez–López, F. Aguilera–Granja, K. Michaelian, A. Vega, Phys. Rev. B 67 (2003) 174413.
[4] F. Aguilera-Granja, A. Vega, Phys. Rev. B 79 (9p) (2009) 144423.
[5] M. Niemeyer, K. Hirsch, V. Zamudio-Bayer, A. Langenberg, M. Vogel, M. Kossick, C. Ebrecht, K. Egashira, A. Terasaki, T. Möller, B.v. Issendorff, J.T. Lau, Phys. Rev. Lett. 108 (5p) (2012), 057201.
[6] F. Aguilera-Granja, Juarez L.F. Da Silva, M.J. Piotrowski, *Eur. J. Phys.* D 67 (7p) (2013) 33.
[7] G. Guzmán-Ramírez, F. Aguilera-Granja, J. Robles, Eur. Phys. Jour. D 57 (2010) 335–342.
[8] R.H. Aguilera-del-Toro, F. Aguilera-Granja, A. Vega, L.C. Balbas, Phys. Chem. Chem. Phys. 16 (2014) 21732–21741.
[9] R.H. Aguilera-del-Toro, F. Aguilera-Granja, A. Vega, C. Balbas, Theo. Chem. Accounts 137 (1–17) (2018) 54.
[10] A.M. Knight, B. Bandyopadhyay, C.L. Anfuso, K.S. Molek, M.A. Duncan, Int. Jour. Mol. Sci. 304 (2011) 29–35.
[11] C.J. Dible, S.T. Akin, S. Ard, C.P. Fowler, M.A. Duncan, J. Phys. Chem. 116 (2012) 2691–2697.
[12] A. García-Prieto, A. Arteche, F. Aguilera-Granja, M.B. Torres, I. Orue, J. Alonso, L. Fernández Barquín, M.L. Fernández-Gubieda, Nanotechnology 26 (10p) (2015) 455703.
[13] Y. Sanchez-Paisal, D. Sanchez-Portal, A. Ayuela, Phys. Rev. B 80 (2009), 045428.
[14] V.W. Brar, R. Decker, H.-M. Solowan, Y. Wang, L. Maserati, K.T. Chan, H. Lee, C. O. Girit, A. Zettl, S.G. Louie, M.L. Cohen, M.F. Crommie, Nat. Phys. 7 (2011) 43–47.
[15] T. Alonso-Lanza, A. Ayuela, F. Aguilera-Granja, ChemPhysChem 16 (2015) 3700–3710.
[16] F. Aguilera-Granja, R. Pis-Diez, J. Nano Res. 18 (12p) (2016) 121.
[17] P. Gambardella, S. Rusponi, M. Veronese, S.S. Dhesi, C. Grazioli, A. Dallmeyer, I. Cabria, R. Zeller, P.H. Dederichs, K. Kern, C. Carbone, H. Brune, Sience 300 (5622) (2003) 1130–1133.
[18] C. Pisani, U. Birkenheuer, Int. J. Quant. Chem. 29 (1995) 221–234.
[19] V. Dupuis, G. Khadra, J.M. Montejano-Carrizales, F. Tournus, F. Aguilera-Granja, A. Tamion, *ACS Applied Nano Materials*, ACS 2 (2019) 2864–2872.
[20] S. Rohart, C. Raufast, L. Favre, E. Bernstein, E. Bonet, V. Dupuis, Phys. Rev. B 74 (7p) (2006) 104408.
[21] A. Bergman, O. Eriksson, Phys. Rev. B 74 (5p) (2006) 104422.
[22] X.Q. An, J.C. Yu, RSC Adv. 1 (2011) 1426–1434.
[23] S. Morales-Torres, L. Pastrana-Martínez, J. Figueiredo, J. Faria, A.T. Silva, Environ. Sci. Pollut. Res. 19 (2012) 3676–3687.
[24] W. Geng, H. Liu, Xiaojun Yao, Phys. Chem. Chem. Phys. 15 (2013) 6025–6034.
[25] B. Bukowski, A. Deskins, Phys. Chem. Chem. Phys. 17 (2015) 29734–29746.
[26] E. Moharramzadeh-Goliaei, N. Seriani, J. Phys. Chem. C 123 (2019) 2855–2863.

[27] M. Lamoth, M. Plodinec, L. Scharfenberg, S. Wrabetz, F. Girgsdies, T. Jones, F. Rosowski, R. Horn, R. Schlogl, E. Frei, ACS Appl. Nano Mater. 2 (2019) 2909–2920.
[28] X.-H. Ning, Q.-L. Meng, Y.-L. Han, D.-Y. Zhou, Li Li, L. Cao, Z.-K. Weng, R. Ding, Z.-B. Wang, RSC Adv. 7 (2017) 34907–34911.
[29] F. Nyongesa, B. Aduda, Adv. Mater. 6 (2017) 31–37.
[30] B. Tang, H. Chen, H. Peng, Z. Wang, W. Huang, Nanomaterials 8 (27p) (2018) 105.
[31] M.P. de Lara-Castells, C. Cabrillo, D.A. Micha, A.O. Mitrushchenkov, T. Vazhappilly, Phys. Chem. Chem. Phys. 20 (2018) 19110–19119.
[32] D.V. Potapenko, Z. Li, R.M. Osgood, J. Phys. Chem. C 119 (2015) 28946–28953.
[33] F. Tumino, P. Carrozzo, L. Mascaretti, C.S. Casari, M. Passoni, S. Tosoni, C. E. Bottani, A. Li Bassi, 2D Mater. 2 (11p) (2015), 045011.
[34] J. Biener, E. Farfan-Arribas, M. Biener, C.M. Friend, R.J. Madix, J. Chem. Phys. 123 (6p) (2005), 094705.
[35] J.M. Soler, E. Artacho, J.D. Gale, A. García, J. Junquera, P. Ordejon, D. Sánchez-Portal, J. Phys. Condens. Matter 14 (2002) 2745–2779.
[36] J.P. Perdew, K. Burke, M. Ernzerhof, Phys. Rev. Lett. 77 (1996) 3865–3868.
[37] N. Troullier, J.L. Martins, Phys. Rev. B 43 (1991) 1993–2006.
[38] L. Kleinman, D.M. Bilander, Phys. Rev. Lett. 48 (1982) 1425–1428.
[39] F. Aguilera-Granja, R.C. Longo, L.J. Gallego, A. Vega, J. Chem. Phys. 132 (8p) (2010) 184507.
[40] T. Alonso-Lanza, A. Ayuela, F. Aguilera-Granja, Phys. Chem. Chem. Phys. 18 (2016) 21913–21920.
[41] F. Aguilera-Granja, A. García-Fuente, A. Vega, Phys. Rev. B 78 (9p) (2008) 134425.
[42] W.H. Press, S.A. Teukolsky, W.T. Vetterling, B.P. Flannery, Numerical Recipes in Fortran, second ed., Cambridge University Press, Cambridge, 1992.
[43] L. Zibordi-Besse, Y. Seminovski, I. Rosalino, D. Guedes-Sobrinho, J.L.F. Da Silva, J. Phys. Chem. C 122 (2018) 27702–27712.
[44] S. Grimme, J. Comput. Chem. 27 (2006) 1787.
[45] P. Giannozzi, et al., J. Phys. Condens. Matter 29 (2017) 465901.
[46] I. Nakamura, H. Mantoku, T. Furukawa, A. Takahashi, T. Fujitani, Surf. Sci. 606 (2012) 1581–1585.
[47] D.T. Boyle, J.A. Wilke, R.M. Palomino, V.H. Lam, D.A. Schlosser, W.J. Andahazy, C.Z. Stopak, D.J. Stacchiola, J.A. Rodriguez, A.E. Baber, J. Phys. Chem. C 121 (2017) 7794–7802.
[48] R.M. Palomino, R.A. Gutíerrez, Z. Liu, S. Tenney, D.C. Grinter, E. Crumlin, I. Waluyo, P.J. Ramírez, J.A. Rodriguez, S.D. Senanayake, ACS Sustain. Chem. Eng. 5 (2017) 10783–11791.